JCTC Journal of Chemical Theory and Computation

Article

pubs.acs.org/JCTC

Mechanistic Insight into Marine Bioluminescence: Photochemistry of the Chemiexcited *Cypridina* (Sea Firefly) Lumophore

Bo-Wen Ding,[†] Panče Naumov,[‡] and Ya-Jun Liu*[,†]

[†]Key Laboratory of Theoretical and Computational Photochemistry, Ministry of Education, College of Chemistry, Beijing Normal University, Beijing 100875, China

[‡]New York University Abu Dhabi, P.O. Box 129188, Abu Dhabi, United Arab Emirates

Supporting Information

ABSTRACT: *Cypridina hilgendorfii* (sea firefly) is a bioluminescent crustacean whose bioluminescence (BL) reaction is archetypal for a number of marine organisms, notably other bioluminescent crustaceans and coelenterates. Unraveling the mechanism of its BL is paramount for future applications of its strongly emissive lumophore. *Cypridina* produces light in a three-step reaction: First, the cypridinid luciferin is activated by an enzyme to produce a peroxide intermediate, cypridinid dioxetanone (CDO), which then decomposes to generate excited oxyluciferin (OxyCLnH*). Finally, OxyCLnH* deexcites to its ground state along with emission of bright blue light. Unfortunately, the detailed mechanism of the critical step, the thermolysis of CDO, remains unknown, and it is unclear whether the light emitter is generated from a neutral form (CDOH) or anionic form (CDO^-) of the CDO precursor. In this work, we investigated the key step in the process by modeling the thermal decompositions of both CDOH and CDO^-. The calculated results indicate that the decomposition of CDO^- occurs via the gradually reversible charge transfer (CT)-initiated luminescence (GRCTIL) mechanism, whereas CDOH decomposes through an entropic trapping mechanism without an obvious CT process. The thermolysis of CDO^- is sensitive to solvent effects and is energetically favorable in polar environments compared with the thermolysis of CDOH. The thermolysis of CDO^- produces the excited oxyluciferin anion ($OxyCLn^-$*), which combines with a proton from the environment to form OxyCLnH*, the actual light emitter for the natural system.

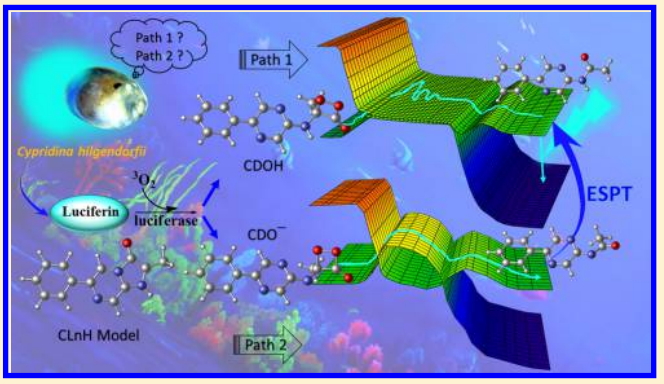

1. INTRODUCTION

Bioluminescence (BL) is one of the most mysterious and visually striking phenomena in nature. Compared with terrestrial bioluminescent creatures such as fireflies, BL is a more commonly utilized means for signaling and communication between marine organisms, particularly bacteria, planktons, coelenterates, and crustaceans.[1,2] The aesthetic effect and applications including real-time in vivo imaging[3,4] and gene reporting[5,6] continue to inspire an exciting (photo)chemistry. With a body length of only 2−3 mm, *Cypridina (Vargula) hilgendorfii*, commonly known as sea firefly, is one of the simplest luminescent marine organisms.[7] It produces extracellular blue BL with an emission maximum at 465 nm.[8] The BL reaction requires only three components: luciferin, luciferase, and oxygen. Unlike many other endocellular BL reactions, additional species such as ATP, magnesium ions, or calcium ions are not required in the *Cypridina* BL, which could be advantageous for some intended applications.[2,9,10] Together with the high BL efficiency (Φ_{BL} = 0.28),[11,12] this turns the *Cypridina* BL into a valuable detection system for active oxygen species[13−18] in biological systems. *Cypridina* BL has already become an indispensable analytical tool in biotechnology and biomedical research, such as enzyme immunoassays,[19−21] imaging,[22−26] quantum-dot-assay-based bioluminescence resonance energy transfer (BRET),[27] immunohistology (IHC),[28] spectroscopy with two-photon fluorescent probes,[29] and monitoring of promoter activity without destroying the cells or tissues.[30−35]

The generally accepted reaction mechanism to describe the BL process of *Cypridina* is presented in Scheme 1. The process consists of three steps:[36−40] (1) In a process catalyzed by luciferase, cypridinid luciferin[41] (CLnH) is oxidized by molecular oxygen, giving a fleeting peroxide intermediate, anionic cypridinid dioxetanone (CDO^-). (2) CDO in anionic form (CDO^-) or neutral form (CDOH) decomposes to generate singlet-excited-state oxyluciferin (OxyCLnH*). (3) OxyCLnH* relaxes to its ground state (S_0), emitting light. The core structure of CLnH is the imidazopyrazine ring (see Scheme 1), which also is the basic structure of coelenterazine, the luciferin of many bioluminescent coelenterates, such as *Aequorea*,[42] *Obelia*,[43] and *Renilla*.[44] Moreover, the three-step BL

Received: October 17, 2014
Published: January 8, 2015

DOI: 10.1021/ct5009203
J. Chem. Theory Comput. 2015, 11, 591−599

Scheme 1. Simplified Three-Step Reaction Mechanism Proposed for *Cypridina* Bioluminescence

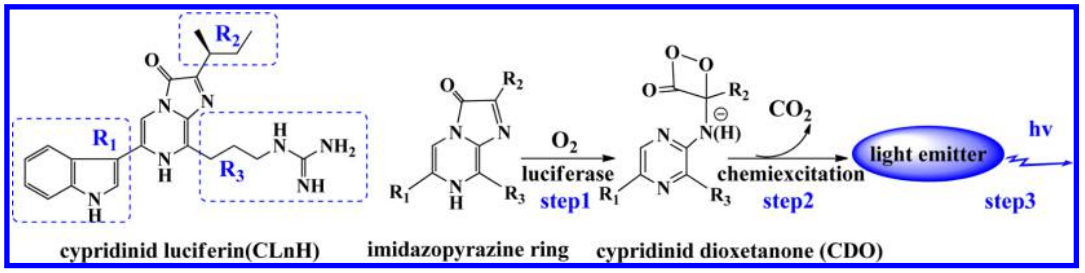

Chart 1. Structures of the Simplified Models of CDOH and CDO^-[a]

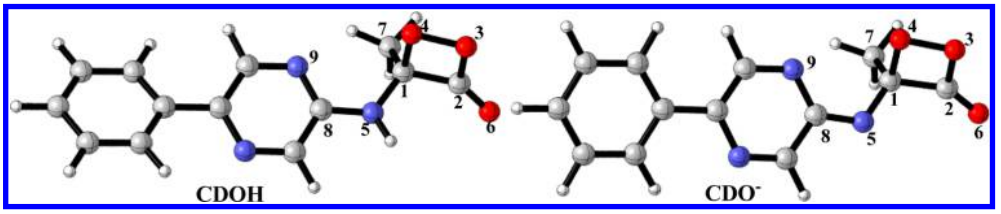

[a]Here and in subsequent illustrations, gray, blue, white, and red balls represent carbon, nitrogen, hydrogen, and oxygen atoms, respectively.

process of *Cypridina* in Scheme 1 is also a general mechanism for many marine organisms, including other crustaceans and coelenterates.[2,7] Therefore, a thorough understanding of the BL mechanism of *Cypridina* is pivotal to explain the BL of other marine organisms. In the critical second step of the BL reaction, the ground-state reactant produces an excited-state product, which emits light. Thus, elucidating the mechanism of the CDO decomposition is paramount to understanding the BL mechanism of many creatures.

1,2-Dioxetanes are important chemiluminescent intermediates in many BL processes, and their neutral and anionic decompositions have been thoroughly investigated by experimental and computational methods. The decomposition of neutral dioxetanes was initially considered as concerted[45] and subsequently as asynchronous-concerted.[46] Recently, a series of density functional theory (DFT) and multireference quantum-chemical calculations indicated that this kind of decomposition reaction occurs through an entropic trapping mechanism.[47−51] On the other hand, the decomposition of anionic dioxetanes is thought to occur via a charge transfer (CT)-initiated luminescence (CTIL) mechanism,[52] which was later replaced by a more accurate model, the gradually reversible CTIL (GRCTIL) mechanism.[50] In addition to CTIL and GRCTIL, the intramolecular CT-induced decomposition (CTID)[53] mechanism was also proposed. Actually, these mechanisms were put forward on the basis of their predecessor, the chemical-initiated electron exchange luminescence (CIEEL) mechanism.[54] CIEEL assumes that the decomposition is initiated by one-electron transfer and a subsequent back electron transfer (BET). The CIEEL mechanism was questioned for the existence and efficiency of the BET process, and the CTIL mechanism was subsequently proposed. CTIL suggests that the decomposition gives an excited-state product via a nonadiabatic transition after the CT process. Later on, the CTID mechanism was advanced; it embraces the essence of CIEEL and the other CT-induced mechanisms, but the CT trend is described as a full one-electron transfer. Further, the GRCTIL mechanism was proposed to describe the chemiexcitation mechanism of anionic firefly dioxetanone, where the CT and back charge transfer (BCT) are gradual and not full one-electron transfer processes and occur in concert with the cleavage of O−O and C−C bonds, respectively. The occurrence of CT was supported experimentally.[55] Moreover, the theoretical predication that the CT and bond cleavage are concerted processes was also confirmed.[56]

However, the detailed mechanism of the decomposition of CDO itself at the molecular and electronic levels remains unknown. Hirano's group investigated the BL mechanism of CDOH analogues with the restricted[39] and unrestricted[57] Becke's three-parameter, Lee−Yang−Parr (B3LYP) methods and found a CTIL decomposition. Ren and co-workers[58] investigated the decompositions of CDO^- and CDOH using a simplified model and the restricted B3LYP functional. First, as pointed out in our previous report,[59] closed-shell DFT failed to describe the decomposition of 1,2-dioxetanone. Second, the B3LYP functional, which employs an improper long-range form of the exchange−correlation functional, may be misleading in regard to the anionic decomposition of 1,2-dioxetanones containing a CT process.[60,61] On the basis of our previous studies of the decomposition of 1,2-dioxetane,[47] 1,2-dioxetanone,[49] firefly dioxetanone,[50] thiazole-substituted dioxetanone,[48] and AMPPD[51] and in order to comprehend the crucial step of *Cypridina* BL, here we investigated in detail the thermolysis of CDOH and CDO^- that leads to the light emitter OxyCLnH* with a suitable functional for these systems. These results add novel insight into the mechanism of *Cypridina* BL.

2. COMPUTATIONAL DETAILS

With a compromise between chemical accuracy and available computational resources, we substituted the larger and flexible structure of the intermediates CDOH and CDO^- with the core skeletons shown in Chart 1, in which R_1, R_2, and R_3 in Scheme 1 have been replaced with phenyl, methyl, and hydrogen, respectively. These substitutions are reasonable and retain the innate characters of both systems, as has been verified previously.[37,38] Although the corresponding models of CDOH and CDO^- were investigated, for simplicity we will use the labels CDOH and CDO^- to represent the two model molecules in the following discussion.

The generally employed functional, B3LYP, underestimates CT excitation energies.[61,62] Here we employed the Coulomb-attenuated hybrid exchange−correlation functional (CAM-

DOI: 10.1021/ct5009203
J. Chem. Theory Comput. 2015, 11, 591−599

B3LYP). This is a new long-range-corrected hybrid exchange−correlation functional proposed by Yanai et al.[63] in 2004 that performs well in predicting CT excitations. For both CDOH and CDO^-, the equilibrium geometry of the reactant (R) was optimized with CAM-B3LYP, while transition state (TS) and intermediate (Int) along the thermolysis reaction coordinate were optimized using the unrestricted form of this functional in cooperation with the broken-symmetry (BS) technology. The BS technology is generally employed to make the initial guess for a biradical by mixing of the HOMO and LUMO. Vibrational analysis was performed for each stationary point to verify whether it is a minimum or a TS. Intrinsic reaction coordination (IRC) calculations were carried out from the geometries of the TSs to confirm that the located TSs actually connect the correct starting and final structures. The energies of several excited states were calculated using LR-TDDFT, which is a conventional time-dependent density functional theory (TDDFT)[64−66] based on the linear response (LR) of S_0 to a time-dependent perturbation. Mulliken population analysis was employed to elucidate the CT characteristics. The 6-31G(d,p) basis set[67,68] was employed for both CAM-B3LYP and TD CAM-B3LYP calculations. The equilibrium geometries of R, TS, and Int were also optimized and the IRC was recalculated in solvent environments. For comparison, two solvents that are generally used in chemiluminescence were taken into consideration: benzene as a nonpolar solvent (dielectric constant ε = 2.25) and DMSO as a polar solvent (ε = 46.70). The polarizable continuum model (PCM)[69,70] was employed for benzene in the self-consistent reaction field calculations, while the conductor-like polarized continuum model (C-PCM)[71] was employed for DMSO. All of the DFT and LR-TDDFT calculations were performed with the Gaussian 09 program.[72]

3. RESULTS AND DISCUSSION

3.1. Chemiluminescence of CDOH. *3.1.1. Potential Energy Curves of the S_0 State.* Under vacuum, three S_0 potential energy curves (PECs) of CDOH were found (Figure 1). Path 1 is an asynchronous-concerted process whose TS (**TS1**) has weak biradical character ($\langle S^2\rangle$ = 0.53) and corresponds to stretching of the O_3-O_4 bond. Path 2 is a synchronous-concerted process whose TS (**TS2**) does not have biradical character ($\langle S^2\rangle$ = 0) and corresponds to simultaneous stretching of both the O_3-O_4 and C_1-C_2 bonds. Path 3 is a stepwise-biradical process that involves two TSs ($\mathbf{TS_{O-O}}$ and $\mathbf{TS_{C-C}}$) and one intermediate (**Int**) with biradical character ($\langle S^2\rangle$ = 0.83, 1.00 and 1.01 for $\mathbf{TS_{O-O}}$, $\mathbf{TS_{C-C}}$, and **Int**, respectively). $\mathbf{TS_{O-O}}$ and $\mathbf{TS_{C-C}}$ correspond to the stretching of the O_3-O_4 and C_1-C_2 bonds, respectively.

The variations of the dominant geometric parameters (the O_3-O_4 and C_1-C_2 bonds and the $O_4-C_1-C_2-O_3$ dihedral angle) along the three reaction paths are displayed in Figure 2. As shown in Figure 2A, the decomposition of CDOH in path 1 starts with the rupture of O_3-O_4. The O_3-O_4 bond is elongated by 0.545 Å from 1.472 to 2.017 Å in **TS1**, while C_1-C_2 remains nearly unchanged (slightly increasing from 1.522 to 1.561 Å; Figure 1.) The C_1-C_2 bond begins to break after TS1, which indicates that the elongation of the O_3-O_4 and C_1-C_2 bonds is asynchronous. In path 2 (Figure 2B), the decomposition commences with the almost synchronous cleavages of the O_3-O_4 and C_1-C_2 bonds via **TS2**. The O_3-O_4 bond is elongated by 0.504 Å in **TS2**, while the C_1-C_2 bond is elongated by 0.141 Å. From the changes in the $O_4-C_1-C_2-O_3$ dihedral angle along the reaction coordinates (Figure 2A,B), the four-membered $O_4-C_1-C_2-O_3$ ring remains planar in the two concerted pathways. According to the Gibbs free energies relative to $\mathbf{R_{CDOH}}$ (ΔG) for CDOH in Figure 1, paths 1 and 2 must climb one TS, overcoming large energy barriers of 30.2 and 31.4 kcal mol^{-1}, respectively. Both of these barriers are unreasonable compared with the experimental measurements on other 1,2-dioxetane and 1,2-dioxetanone derivatives, whose reaction barriers are about 20.0 kcal mol^{-1} (for details, see the Supporting Information for ref 50). Therefore, the two paths should be excluded.

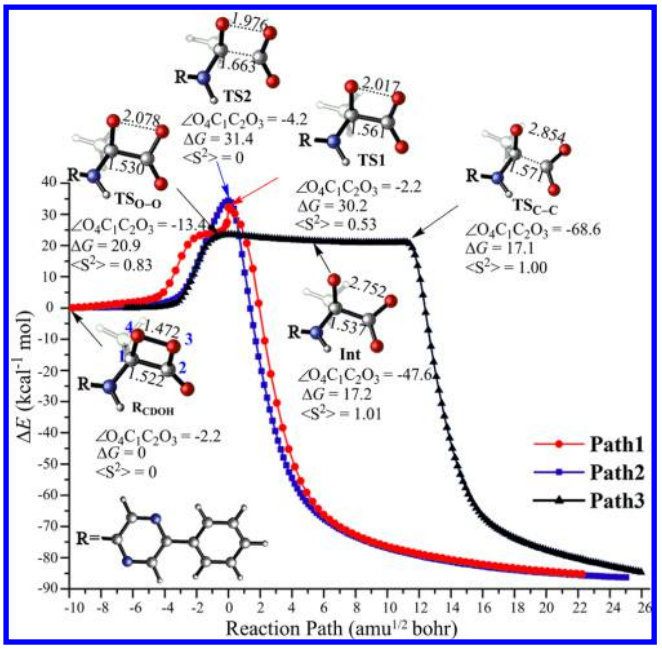

Figure 1. S_0 PECs of CDOH computed at the UCAM-B3LYP/6-31G(d,p) level. (Units: Å for bond lengths, deg for dihedral angles, and kcal mol^{-1} for ΔG.)

On the other hand, as the breaking of the O_3-O_4 bond is the rate-determining step in path 3, in agreement with experiment,[73] $\mathbf{R_{CDOH}}$ needs to overcome an activation barrier of only 20.9 kcal mol^{-1}. In path 3 (Figure 2C), the decomposition of CDOH commences with rupture of the O_3-O_4 bond followed by rupture of the C_1-C_2 bond. The O_3-O_4 bond length in $\mathbf{TS_{O-O}}$ is 2.078 Å (Figure 1), which is 0.606 Å longer than that in the reactant, but the C_1-C_2 bond length changes little in going from the reactant to $\mathbf{TS_{O-O}}$ (from 1.522 to 1.530 Å). The O_3-O_4 and C_1-C_2 bond lengths are 2.752 and 1.537 Å in **Int** and 2.854 and 1.571 Å in $\mathbf{TS_{C-C}}$, respectively, which implies that the O_3-O_4 bond is broken completely in **Int** and the C_1-C_2 bond gradually breaks after **Int**. Thus, the ruptures of the O_3-O_4 and C_1-C_2 bonds occur sequentially. In addition, the $O_4-C_1-C_2-O_3$ dihedral angle is −13.4, −47.6, and −68.6° in $\mathbf{TS_{O-O}}$, **Int**, and $\mathbf{TS_{C-C}}$, respectively, which indicates that the four atoms deviate from the plane of the four-membered ring as the reaction proceeds. We can therefore infer that the decomposition process of the stepwise pathway as follows: In the initial stage, the weak O_3-O_4 bond is elongated, but the C_1-C_2 bond length remains nearly unchanged. After the O_3-O_4 bond is completely broken in the vicinity of **Int**, the C_1-C_2 bond starts to elongate, resulting in the final departure of a carbon dioxide molecule to form the products.

3.1.2. Chemiluminescent Decomposition Pathway of CDOH. As mentioned above, path 3 is energetically favorable

DOI: 10.1021/ct5009203
J. Chem. Theory Comput. 2015, 11, 591−599

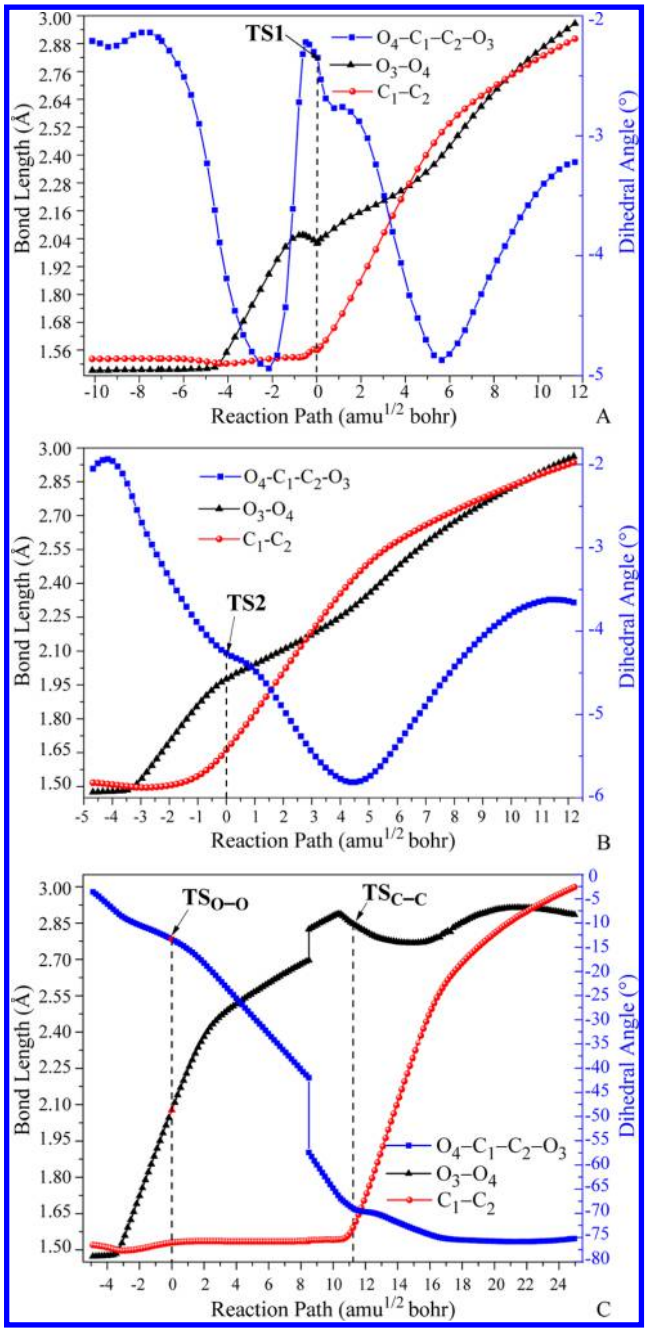

Figure 2. Changes of C_1–C_2 and O_3–O_4 (Å), and O_4–C_1–C_2–O_3 (deg) along the three pathways of CDOH decomposition (path 1: A, path 2: B, path 3: C) computed at the UCAM-B3LYP/6-31G(d,p) level.

compared with the other two paths. Below we analyze the detailed mechanism of CDOH decomposition in path 3 on the basis of the S_0 and S_1 PECs along the decomposition process. Figure 3 shows the approximate diabatic PECs for CDOH decomposition based on the corrected adiabatic PECs of the S_0 and S_1 states (shown in the inset) obtained by connecting electronic states with the same transition characteristics. The natural orbitals (NOs) of some important points along the decomposition process of CDOH for the S_0 and S_1 states are collected in Table S1 in the Supporting Information (SI)

According to the NO analysis in Table S1, the S_0 state of CDOH near the $\mathbf{R}_{CDOH}$ region mainly features a Hartree–Fock closed-shell configuration in which all of the bonding and

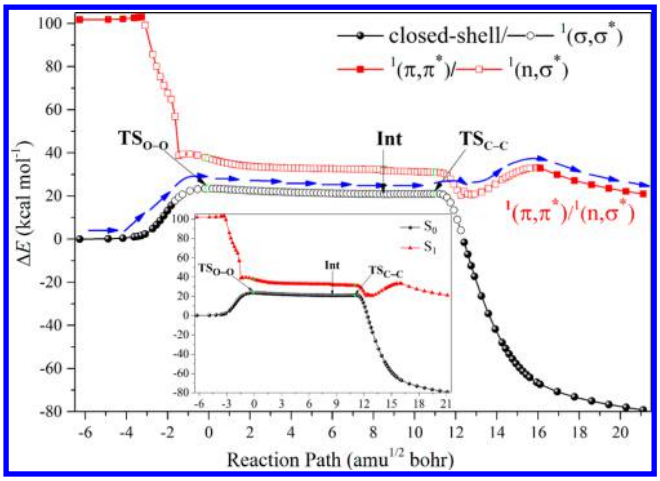

Figure 3. Adiabatic PECs of the S_0 and S_1 states (inset) and the approximate diabatic PECs of the $^1(\sigma,\sigma^*)$, $^1(n,\sigma^*)$, and $^1(\pi,\pi^*)$ configurations of CDOH decomposition computed at the TD UCAM-B3LYP/6-31G(d,p) level.

nonbonding orbitals are doubly occupied. The S_1 state near the $\mathbf{R}_{CDOH}$ region corresponds to the $\pi \rightarrow \pi^*$ transition, where π represents the pπ-conjugated orbital comprising the π orbitals of the pyrazine and benzene rings and the p orbital of N_5 and π^* represents the π-antibonding orbital of the pyrazine ring. The S_0 state takes on (σ,σ^*) character gradually, and the S_1 state changes from the $^1(\pi,\pi^*)$ configuration to a $^1(n,\sigma^*)$ configuration along with elongation of the O_3–O_4 bond. Here n refers to the in-plane p orbital of O_3 and the out-of-plane p orbital of O_4. After the complete rupture of the C_1–C_2 bond, the characteristic of S_0 returns to the closed-shell configuration, while S_1 returns to the $^1(\pi,\pi^*)$ configuration at IRC = 16.102 amu$^{1/2}$ bohr. Here, π is also the pπ-conjugated orbital of the pyrazine and benzene rings and N_5, but π^* is composed of the π-antibonding orbital of pyrazine and the C_1–O_4 carbonyl. Thus, in Figure 3 the S_0 and S_1 states are denoted as closed-shell/$^1(\sigma,\sigma^*)$ and $^1(\pi,\pi^*)/^1(n,\sigma^*)$, respectively.

As shown in Figure 3, the S_0 and S_1 adiabatic PECs are flat from IRC = −0.909 to 11.910 amu$^{1/2}$ bohr. The flat region between $\mathbf{TS}_{O-O}$ (with a barrier of 20.9 kcal mol^{-1}) and $\mathbf{TS}_{C-C}$ (with a barrier of 17.1 kcal mol^{-1}) indicates a nearly barrierless process, as the entropy effects become very significant in this region. The entropic trapping mechanism forces the molecule to spend a "long" time exploring the PES.[74−77] According to the NO analysis (Table S1) and $\langle S^2 \rangle$ analysis (Figure S2A), in the flat region the S_0 state has typical biradical character and presents a (σ,σ^*) characteristic, while the main characteristic of the S_1 state is $^1(n,\sigma^*)$. The smallest energy gap between the two PECs is 9.9 kcal mol^{-1} at IRC = 11.242 amu$^{1/2}$ bohr. Higher-level calculations will surely predict an even smaller energy gap between the two PECs in the flat region.[47−51] The importance of including multireference correlation for these kind of systems has been well-elucidated.[78−80] This implies that the $^1(\sigma,\sigma^*)$ and $^1(n,\sigma^*)$ configurations become nearly degenerate in the flat biradical region. The considerable energetic error in the nearly degenerate biradical region may come from spin contamination of the reference state introduced by the BS technology[50] (for the energetic errors and the improvement of LR-TDDFT on biradical systems, see the SI). Anyway, the flat nearly degenerate region imparts nonadiabatic transitions with infinite possibilities arousing surface hopping between $^1(\sigma,\sigma^*)$ and $^1(n,\sigma^*)$ configurations,

DOI: 10.1021/ct5009203
J. Chem. Theory Comput. 2015, 11, 591−599

which is similar to our previous theoretical studies.[50,51] After the nearly degenerate region, the CDOH molecule has two choices: to continue on the $^1(\sigma,\sigma^*)$ potential energy surface (PES) to form ground-state CO_2 and OxyCLnH as products or to jump to the $^1(n,\sigma^*)$ PES to produce ground-state CO_2 and excited-state OxyCLnH*, namely, the light emitter.

The populations of Mulliken charges on the CO_2 and OxyCLnH moieties (Figure 4) show that no obvious CT and

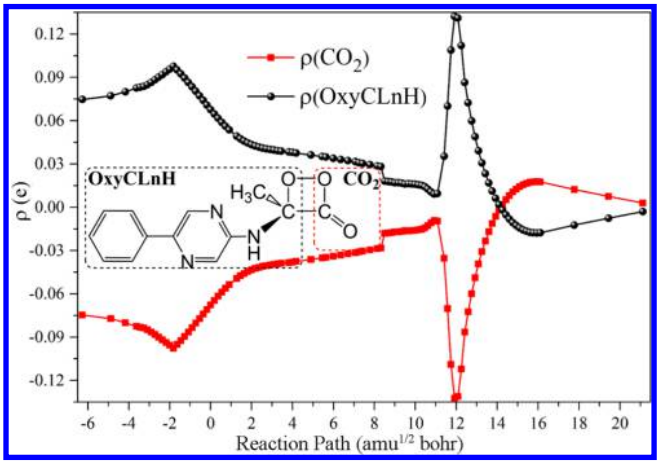

Figure 4. Populations of Mulliken charges on the CO_2 and OxyCLnH moieties in the decomposition of CDOH (path 3) along the IRC under vacuum calculated at the UCAM-B3LYP/6-31G(d,p) level.

BCT processes arise during the decomposition of CDOH. Therefore, the chemiluminescence process of CDOH can be interpreted in terms of the entropic trapping mechanism, which is in line with our previous multireference-calculated conclusion on the neutral dioxetanones.[50]

3.1.3. Solvent Effects on CDOH Chemiluminescent Decomposition. In order to understand the solvent effects on the chemiluminescent decomposition of CDOH, the above stationary points ($\mathbf{R_{CDOH}}$, **Int**, $\mathbf{TS_{O-O}}$, and $\mathbf{TS_{C-C}}$ in path 3) were reoptimized in polar (DMSO) and nonpolar (benzene) solvents at the same theoretical level as under vacuum. The dominant geometric parameters and the values of ΔG and $\langle S^2\rangle$ for these stationary points along path 3 of CDOH in the two solvents are summarized in Table S3. The $\langle S^2\rangle$ values of the two TSs and **Int** show that the decompositions of CDOH in DMSO and benzene have biradical character. Comparison of the dominant geometric parameters in Figure 1 with the corresponding ones in Table S3 shows that the solvents affect the $O_4-C_1-C_2-O_3$ dihedral angle but have little influence on the bond lengths. The $O_4-C_1-C_2-O_3$ dihedral angle is twisted by 66.4, 62.9, and 34.8° in $\mathbf{TS_{C-C}}$ relative to $\mathbf{R_{CDOH}}$ under vacuum, in benzene, and in DMSO, respectively. The reaction barriers from $\mathbf{R_{CDOH}}$ to $\mathbf{TS_{O-O}}$ without CT characteristics are 20.9, 21.0, and 21.0 kcal mol^{-1} under vacuum, in benzene, and in DMSO, respectively, which indicates that the solvents have little impact on the decomposition process of CDOH.

Figure S3 shows a comparison of the S_0 PECs of CDOH under vacuum, in benzene, and in DMSO calculated using UCAM-B3LYP functional. It can be concluded that the two solvents hardly affect the non-CT S_0 PEC of CDOH, in agreement with our multireference studies on the neutral form of firefly dioxetanone.[50] We note that the energy of the S_0 state in DMSO is obviously lower than those in benzene and under vacuum after the rupture of the C_1-C_2 bond. This may be due to the increased solvent polarity, which induces CT character in the S_0 state after $\mathbf{TS_{C-C}}$ (see the details in the following discussion of the charge populations for the CDOH decomposition in the two solvents.).

Comparing the charge distributions in DMSO and benzene (Figure 5) with that under vacuum (Figure 4), we find that a

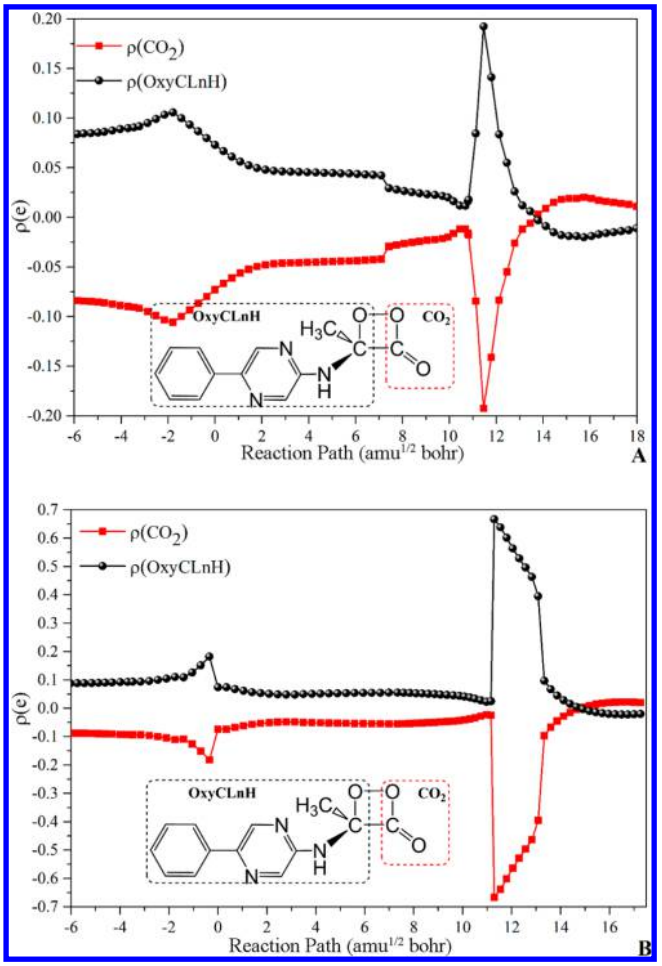

Figure 5. Populations of Mulliken charges on the CO_2 and OxyCLnH moieties in the decomposition of CDOH (path 3) along the IRC in (A) benzene and (B) DMSO calculated at the UCAM-B3LYP/6-31G(d,p) level.

bigger dielectric constant of the solvent allows the solvent to facilitate the charge separation more easily. Thus, in a polar solvent (DMSO), the S_0 state takes the obvious CT character in the vicinity of $\mathbf{TS_{C-C}}$ compared with that under vacuum and in a nonpolar solvent (benzene).

3.2. Chemiluminescence of CDO^-. *3.2.1. The S_0 PEC.* For the decomposition of CDO^-, a concerted pathway was explored, as described in Figure 6A. According to the variations of dominant geometric parameters in Figure 6B, the decomposition of CDO^- also starts with breaking of the O_3-O_4 bond. Although the variation trends of the O_3-O_4 and C_1-C_2 bond lengths of CDO^- are similar to those of CDOH (path 3), only one TS ($\mathbf{TS_{O-O}}$) was located on the S_0 PES. $\mathbf{TS_{O-O}}$ also has biradical character ($\langle S^2\rangle$ = 0.52; Figure 6A). The reactant $\mathbf{R_{CDO^-}}$ has an O_3-O_4 bond length of 1.471 Å and a C_1-C_2 bond length of 1.521 Å. As the reaction proceeds, the O_3-O_4 bond is elongated to 1.825 Å in $\mathbf{TS_{O-O}}$, but the C_1-C_2 bond length does not vary appreciably (from 1.521 to 1.524 Å).

DOI: 10.1021/ct5009203
J. Chem. Theory Comput. 2015, 11, 591−599

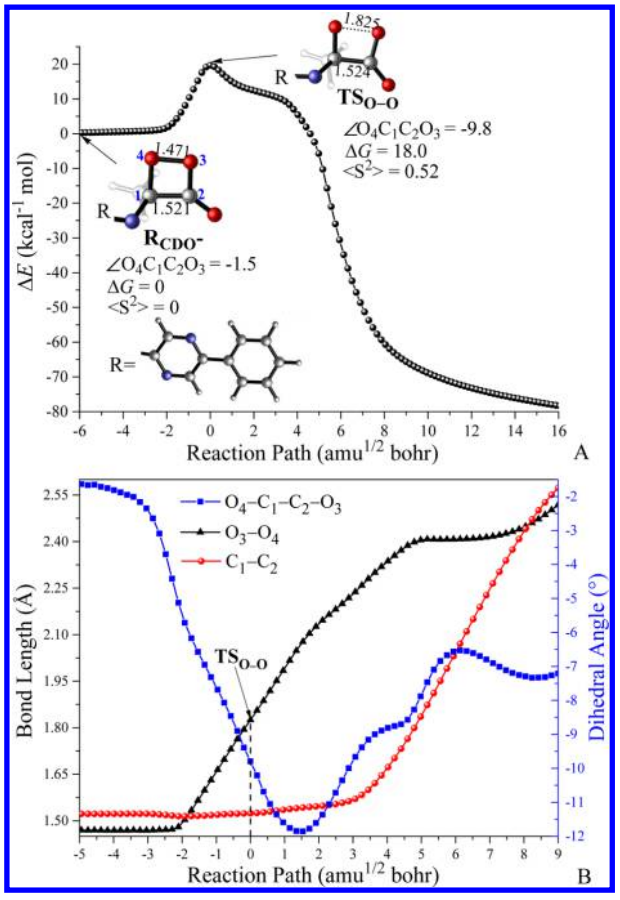

Figure 6. (A) S_0 PEC of CDO^- and (B) changes in the C_1-C_2 and O_3-O_4 bond lengths and the $O_4-C_1-C_2-O_3$ dihedral angle in the S_0 state computed at the UCAM-B3LYP/6-31G (d,p) level. (Units: Å for bond lengths, deg for dihedral angles, and kcal mol^{-1} for ΔG.)

Therefore, the dissociation of the C_1-C_2 and O_3-O_4 bonds is an asynchronous process. The change in the $O_4-C_1-C_2-O_3$ dihedral angle, which first decreases from −2.0 to −12.0° and then increases to −7.0° after complete cleavage of the C_1-C_2 bond (Figure 6B), shows that the twisting mode barely contributes to the bond dissociation. Therefore, the decomposition of CDO^- is a planar asynchronous-concerted process. In addition, the reaction barrier for CDO^- (18.0 kcal mol^{-1}) is 2.9 kcal mol^{-1} smaller than that for CDOH, so the S_0 PEC of CDO^- is the energetically more feasible pathway for *Cypridina* BL from the viewpoint of thermodynamics.

3.2.2. Chemiluminescence Pathway of CDO^-. The chemiluminescent PECs of CDO^- are depicted in Figure 7. Similar to CDOH, near the ground state $\mathbf{R}_{CDO^-}$, the S_0 and S_1 states of CDO^- mainly have closed-shell/$^1(\sigma,\sigma^*)$ and $^1(\pi,\pi^*)/^1(\pi,\sigma^*)$ characteristics, respectively (Table S2). Here π represents the pπ-conjugated orbital of the pyrazine ring and N_5, and π^* represents the π-antibonding orbital of the pyrazine ring. Unlike CDOH, the S_0 state of CDO^- changes to a $^1(\pi,\sigma^*)$ configuration along with stretching of the O_3-O_4 bond because the π^* orbital couples with the σ^* orbital of the O_3-O_4 bond. The S_1 state changes from $^1(\pi,\sigma^*)$ to a $^1(\sigma,\sigma^*)$ configuration at IRC = −0.192 amu$^{1/2}$ bohr. When the C_1-C_2 bond break completely, the S_1 state returns to the $^1(\pi,\pi^*)$ configuration and the S_0 state to the closed-shell configuration. Thus, we use the closed-shell/$^1(\sigma,\sigma^*)$ and $^1(\pi,\sigma^*)$ configurations to represent the S_0 state and $^1(\pi,\pi^*)/^1(\pi,\sigma^*)$ and $^1(\sigma,\sigma^*)$ configurations to represent the S_1 state.

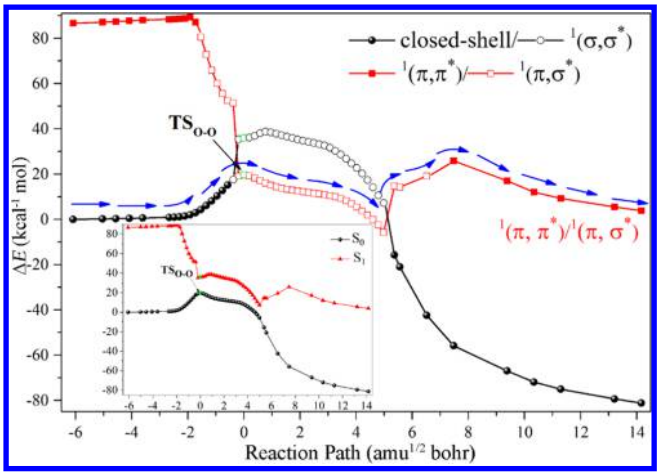

Figure 7. Adiabatic PECs of the S_0 and S_1 states (inset) and the approximate diabatic PECs of the $^1(\sigma,\sigma^*)$, $^1(\pi,\pi^*)$, and $^1(\pi,\sigma^*)$ configurations for CDO^- decomposition computed at the TD UCAM-B3LYP/6-31G (d,p) level.

From the adiabatic PECs of S_0 and S_1 in the Figure 7 inset, it can be observed that the S_0 and S_1 PECs are close to each other when the C_1-C_2 and O_3-O_4 bonds undergo cleavage. This implies that the S_0 and S_1 PESs may twice intersect with each other at the two regions. The smallest energy gaps are 16.2 and 12.9 kcal mol^{-1} at IRC = −0.192 and 4.981 amu$^{1/2}$ bohr, respectively. From the NOs (Table S2) and the $\langle S^2\rangle$ values of every point (Figure S2B), S_0 takes on biradical $^1(\pi,\sigma^*)$ character and S_1 presents a $^1(\sigma,\sigma^*)$ configuration in the regions near IRC = −0.192 and 4.981 amu$^{1/2}$ bohr. From the diabatic PECs of CDO^-, the double crossing between the $^1(\sigma,\sigma^*)$ and $^1(\pi,\sigma^*)$ PESs can be clearly seen. Unfortunately, the currently employed method does not have the capability to optimize the geometries of the two crossing points, and the multireference methods cannot handle such a large system. Similar to our previously studied 1,2-dioxetanone anions,[50,51] the double crossing renders an effective nonadiabatic transition between the $^1(\pi,\sigma^*)$ and $^1(\sigma,\sigma^*)$ configurations for surface hopping from the S_0 PES to the S_1 PES and then produces ground-state CO_2 and excited-state $OxyCLn^-$ ($OxyCLn^-$*) as products. However, $OxyCLn^-$* is not the light emitter for the natural system. The actual light emitter for *Cypridina* is OxyCLnH*, as evidenced by our combined experimental and theoretical study.[40] Because $OxyCLn^-$* is strongly basic, it easily combines with a proton from the environment to form OxyCLnH* via excited-state proton transfer. Obelin bioluminescence has a similar process.[81]

The Mulliken charge populations (Figure 8) show that there is a gradual CT process in the CDO^- decomposition. The value of $\rho(OxyCLn^-)$ gradually decreases from −0.83e to −0.41e while $\rho(CO_2)$ gradually increases from −0.17e to −0.59e with dissociation of the O_3-O_4 bond along the reaction coordinate from −6.086 to 3.449 amu$^{1/2}$ bohr. This corresponds to CT from the $OxyCLn^-$ moiety to the CO_2 moiety. The value of $\rho(OxyCLn^-)$ increases gradually from −0.42e to −0.99e while $\rho(CO_2)$ gradually decreases from −0.58e to −0.02e along the IRC from 3.641 to 14.163 amu$^{1/2}$ bohr. This corresponds to BCT from the CO_2 moiety to the $OxyCLn^-$ moiety. Both the CT and the BCT are gradual, which means that the CT and the O_3-O_4 bond cleavage are concerted and that the BCT and the

DOI: 10.1021/ct5009203
J. Chem. Theory Comput. 2015, 11, 591−599

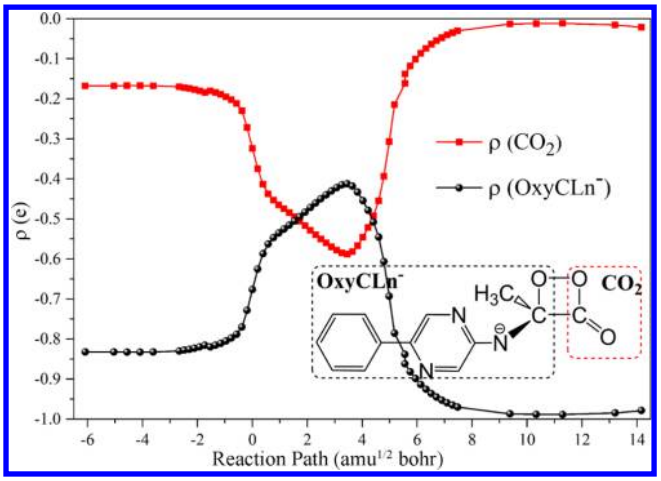

Figure 8. Populations of Mulliken charges on the CO_2 and $OxyCLn^-$ moieties along the decomposition reaction pathway of CDO^- under vacuum calculated at the UCAM-B3LYP/6-31G(d,p) level.

C_1-C_2 bond cleavage are also concerted. The two concerted processes are required for efficient chemiluminescence and have been evidenced by experiments.[56] Besides, both the CT and the BCT are partial rather than full electron transfers. The variations in the electronic structure, especially the double crossing between the S_0 and S_1 PESs, are consistent with those of firefly dioxetanone anion calculated by the CASPT2 method.[50] Therefore, the chemiluminescent decomposition of CDO^- cannot be described by the intramolecular CIEEL mechanism. Instead, it can be elaborated by the GRCTIL mechanism (for details, see ref 50): the chemiluminescence of CDO^- commences with a CT then a subsequent BCT along with the separation of CO_2 and $OxyCLn^-$*.

3.2.3. Solvent Effects on CDO^- Decomposition. The geometric structures of the stationary points of CDO^- ($\mathbf{R}_{CDO^-}$ and $\mathbf{TS}_{O-O}$) were also reoptimized in DMSO and benzene. Their key parameters are shown in Table S4. The values of $\langle S^2 \rangle$ for $\mathbf{TS}_{O-O}$ are 0.41 and 0.46 in DMSO and benzene, respectively, which shows that both of them exhibit biradical characteristics like those under vacuum. Comparison of the O_3-O_4 and C_1-C_2 bond lengths and $O_4-C_1-C_2-O_3$ dihedral angles in Figure 6A with the corresponding ones in Table S4 shows that the solvents do not affect the geometric structural changes in the decomposition of CDO^-. The reaction barriers from $\mathbf{R}_{CDO^-}$ to $\mathbf{TS}_{O-O}$ of the CT characteristic are 18.0, 16.5, and 16.0 kcal mol^{-1} under vacuum, in benzene and in DMSO, respectively, which indicates that the CDO^- tends to decompose in the solvent with the bigger dielectric constant.

A comparison of the S_0 PECs of CDO^- under vacuum, in benzene, and in DMSO is displayed in Figure S4. It is obvious that the current two solvents make some difference in the energies of the S_0 PEC in the biradical CT region and have almost no effect on the closed-shell non-CT region for CDO^-. Especially, the current solvents decrease the reaction energies in the BCT region. These show that the solvent has an effect on the CT state.

From the Mulliken charge populations of CDO^- in Figures 8 and S5, there is a common trend of gradual CT and BCT along the reaction coordinate in the two solvents, similar to that under vacuum. The difference is in the amounts of transferred charge, which are about 0.42e, 0.48e, and 0.53e under vacuum, in benzene, and in DMSO, respectively. This means that an increase in the dielectric constant of the solvent is favorable for CT from the $OxyCLn^-$ moiety to the CO_2 moiety and stabilization of the CT state.

4. CONCLUSIONS

The bioluminescence mechanism of *Cypridina* has not been well understood experimentally and theoretically. The biggest challenge is to elucidate the decomposition mechanism of CDO. The decomposition process involves a biradical, nearly degenerate states, and the CT phenomenon. In this work, we studied the decomposition processes of the neutral and anionic CDO using the CAM-B3LYP method. Although three possible decomposition pathways were located for CDOH, the stepwise-biradical pathway appears to be the most feasible one because of its low reaction barrier. The two TSs and one intermediate in the biradical pathway all have obvious biradical characteristics and very similar energies. The flat region on the PES indicates an entropic trapping mechanism. The nearly degenerate PESs of the S_0 and S_1 states in the long flat region give infinite possibilities for nonadiabatic transitions, which result in the excited-state product, the light emitter for CDOH chemiluminescence. The thermolysis of CDO^- is an asynchronous-concerted process with only one biradical TS. The double crossing between the $^1(\sigma,\sigma^*)$ and $^1(\pi,\sigma^*)$ PESs provides an effective nonadiabatic transition from the S_0 state to the S_1 state in the chemiluminescence of CDO^-. The chemiluminescent decomposition of CDO^- includes a gradual CT and a subsequent BCT with the formation of excited products, which is similar to that in decompositions of other 1,2-dioxetanone derivatives and can be also explicated by the GRCTIL mechanism. In terms of thermodynamics, CDO^- is preferred over CDOH in the *Cypridina* bioluminescence; the present calculations indicate that it is the decomposition of CDO^- that leads the *Cypridina* BL, although the actual light emitter is neutral. The solvent has a scarce effect on CDOH because of the non-CT process. However, the polarity of the solvent may obviously enhance the chemiexcitation of CDO^- by stabilizing the CT states.

■ ASSOCIATED CONTENT

Supporting Information

Natural orbitals and occupation numbers calculated by the CAM-B3LYP method; S_0 PECs and variations in the Mulliken charge populations and important geometrical parameters at the CAM-B3LYP level along the IRCs of CDOH and CDO^- under vacuum, in benzene, and in DMSO; correction of the spin contamination of the S_0 and S_1 PECs of CDOH and CDO^- under vacuum; and Cartesian coordinates for all of the stationary points in CDOH and CDO^- decomposition. This material is available free of charge via the Internet at http://pubs.acs.org.

■ AUTHOR INFORMATION

Corresponding Author

*E-mail: yajun.liu@bnu.edu.cn.

Funding

This study was supported by the National Natural Science Foundation of China (Grants 21273021, 21325312, and 21421003) and the Major State Basic Research Development Program (Grant 2011CB808500).

Notes

The authors declare no competing financial interest.

DOI: 10.1021/ct5009203
J. Chem. Theory Comput. 2015, 11, 591−599

REFERENCES

(1) Teranishi, K. *Bioorg. Chem.* **2007**, *35*, 82−111.
(2) Goto, T. *Pure Appl. Chem.* **1968**, *17*, 421−442.
(3) van Oosten, M.; Schäfer, T.; Gazendam, J. A. C.; Ohlsen, K.; Tsompanidou, E.; de Goffau, M. C.; Harmsen, H. J. M.; Crane, L. M. A.; Lim, E.; Francis, K. P.; Cheung, L.; Olive, M.; Ntziachristos, V.; van Dijl, J. M.; van Dam, G. M. *Nat. Commun.* **2013**, *4*, No. 2584.
(4) Zhang, L.; Xu, F.; Chen, Z.; Zhu, X.; Min, W. *J. Phys. Chem. Lett.* **2013**, *4*, 3897−3902.
(5) Dothager, R. S.; Flentie, K.; Moss, B.; Pan, M.-H.; Kesarwala, A.; Piwnica-Worms, D. *Curr. Opin. Biotechnol.* **2009**, *20*, 45−53.
(6) Cui, L.; Zhong, Y.; Zhu, W.; Xu, Y.; Du, Q.; Wang, X.; Qian, X.; Xiao, Y. *Org. Lett.* **2011**, *13*, 928−931.
(7) Shimomura, O. *J. Microsc.* **2005**, *217*, 3−15.
(8) Shimomura, O.; Johnson, F. H.; Masugi, T. *Science* **1969**, *164*, 1299−1300.
(9) McCapra, F. *Acc. Chem. Res.* **1976**, *9*, 201−208.
(10) McCapra, F. *Proc. R. Soc. London, Ser. B* **1982**, *215*, 247−272.
(11) Johnson, F. H.; Shimomura, O.; Saiga, Y.; Gershman, L. C.; Reynolds, G. T.; Waters, J. R. *J. Cell. Comp. Physiol.* **1962**, *60*, 85−103.
(12) Shimomura, O.; Johnson, F. H. *Photochem. Photobiol.* **1970**, *12*, 291−295.
(13) Mahé, É.; Bornoz, P.; Briot, E.; Chevalet, J.; Comninellis, C.; Devilliers, D. *Electrochim. Acta* **2013**, *102*, 259−273.
(14) Takeshita, K.; Okazaki, S.; Itoda, A. *Anal. Chem.* **2013**, *85*, 6833−6839.
(15) Jiang, Z.; Chen, M.; Hu, Y.; Wang, J.; Chen, G. *Luminescence* **2013**, *28*, 922−926.
(16) Bancirova, M. *Luminescence* **2011**, *26*, 685−688.
(17) Sekiya, M.; Umezawa, K.; Sato, A.; Citterio, D.; Suzuki, K. *Chem. Commun.* **2009**, 3047−3049.
(18) Osman, A. M.; Laane, C.; Hilhorst, R. *Luminescence* **2001**, *16*, 45−50.
(19) Wu, C.; Irie, S.; Yamamoto, S.; Ohmiya, Y. *Luminescence* **2009**, *24*, 131−133.
(20) Wu, C.; Kawasaki, K.; Ogawa, Y.; Yoshida, Y.; Ohgiya, S.; Ohmiya, Y. *Anal. Chem.* **2007**, *79*, 1634−1638.
(21) Mitani, M.; Yokoyama, Y.; Ichikawa, S.; Sawada, H.; Matsumoto, T.; Fujimori, K.; Kosugi, M. *J. Biolumin. Chemilumin.* **1994**, *9*, 355−361.
(22) Wu, C.; Mino, K.; Akimoto, H.; Kawabata, M.; Nakamura, K.; Ozaki, M.; Ohmiya, Y. *Proc. Natl. Acad. Sci. U.S.A.* **2009**, *106*, 15599−15603.
(23) Maguire, C. A.; Bovenberg, M. S.; Crommentuijn, M. H. W.; Niers, J. M.; Kerami, M.; Teng, J.; Sena-Esteves, M.; Badr, C. E.; Tannous, B. A. *Mol. Ther.—Nucleic Acids* **2013**, *2*, No. e99.
(24) Bovenberg, M. S.; Degeling, M. H.; Hejazi, S.; Amante, R. J.; van Keulen, M.; Jeuken, J. W.; Akbaripanahi, S.; Vleggeert-Lankamp, C. L.; Tannous, M.; Wesseling, P.; Wurdinger, T.; Tannous, B. A. *Anal. Chem.* **2013**, *85*, 10205−10210.
(25) He, Y.; Xing, D.; Tan, S.; Tang, Y.; Ueda, K. *Phys. Med. Biol.* **2002**, *47*, 1535−1541.
(26) Inouye, S.; Ohmiya, Y.; Toya, Y.; Tsuji, F. I. *Proc. Natl. Acad. Sci. U.S.A.* **1992**, *89*, 9584−9587.
(27) Wu, C.; Kawasaki, K.; Ohgiya, S.; Ohmiya, Y. *Photochem. Photobiol. Sci.* **2011**, *10*, 1531−1534.
(28) Wu, C.; Wang, K.-Y.; Guo, X.; Sato, M.; Ozaki, M.; Shimajiri, S.; Ohmiya, Y.; Sasaguri, Y. *Luminescence* **2013**, *28*, 38−43.
(29) Sun, Y.; Liu, X.-T.; Guo, J.-F.; Ren, A.-M.; Wang, D. *J. Phys. Org. Chem.* **2013**, *26*, 822−833.
(30) Yamada, Y.; Nishide, S. Y.; Nakajima, Y.; Watanabe, T.; Ohmiya, Y.; Honma, K.; Honma, S. *Anal. Biochem.* **2013**, *439*, 80−87.
(31) Ochi, Y.; Sugawara, H.; Iwami, M.; Tanaka, M.; Eki, T. *Yeast* **2011**, *28*, 265−278.
(32) Tanimura, M.; Watanabe, N.; Ijuin, H. K.; Matsumoto, M. *J. Org. Chem.* **2010**, *75*, 3678−3684.
(33) Tochigi, Y.; Sato, N.; Sahara, T.; Wu, C.; Saito, S.; Irie, T.; Fujibuchi, W.; Goda, T.; Yamaji, R.; Ogawa, M.; Ohmiya, Y.; Ohgiya, S. *Anal. Chem.* **2010**, *82*, 5768−5776.
(34) Xu, W.; Wei, Y.; Xing, D.; Chen, Q. *Anal. Sci.* **2008**, *24*, 115−119.
(35) Yamagishi, K.; Enomoto, T.; Ohmiya, Y. *Anal. Biochem.* **2006**, *354*, 15−21.
(36) McCapra, F.; Chang, Y. C. *Chem. Commun.* **1967**, 1011−1012.
(37) Kondo, H.; Igarashi, T.; Maki, S.; Niwa, H.; Ikeda, H.; Hirano, T. *Tetrahedron Lett.* **2005**, *46*, 7701−7704.
(38) Takahashi, Y.; Kondo, H.; Maki, S.; Niwa, H.; Ikeda, H.; Hirano, T. *Tetrahedron Lett.* **2006**, 6057−6061.
(39) Hirano, T.; Takahashi, Y.; Kondo, H.; Maki, S.; Kojima, S.; Ikeda, H.; Niwa, H. *Photochem. Photobiol. Sci.* **2008**, *7*, 197−207.
(40) Naumov, P.; Wu, C.; Liu, Y. J.; Ohmiya, Y. *Photochem. Photobiol. Sci.* **2012**, *11*, 1151−1155.
(41) Morin, J. G. *Luminescence* **2011**, *26*, 1−4.
(42) Chen, S.-F.; Ferré, N.; Liu, Y.-J. *Chem.—Eur. J.* **2013**, *19*, 8466−8472.
(43) Chen, S.; Navizet, I.; Lindh, R.; Liu, Y.; Ferré, N. *J. Phys. Chem. B* **2014**, *118*, 2896−2903.
(44) Stepanyuk, G. A.; Liu, Z.-J.; Markova, S. S.; Frank, L. A.; Lee, J.; Vysotski, E. S.; Wang, B.-C. *Photochem. Photobiol. Sci.* **2008**, *7*, 442−447.
(45) Turro, N. J.; Lechtken, P. *J. Am. Chem. Soc.* **1973**, *95*, 264−266.
(46) Adam, W.; Baader, W. J. *J. Am. Chem. Soc.* **1985**, *107*, 410−416.
(47) Vico, L. D.; Liu, Y.-J.; Krogh, J. W.; Lindh, R. *J. Phys. Chem. A* **2007**, *111*, 8013−8019.
(48) Liu, F.; Liu, Y.-J.; Vico, L. D.; Lindh, R. *Chem. Phys. Lett.* **2009**, *484*, 69−75.
(49) Liu, F.; Liu, Y.-J.; Vico, L. D.; Lindh, R. *J. Am. Chem. Soc.* **2009**, *131*, 6181−6188.
(50) Yue, L.; Liu, Y.-J.; Fang, W.-H. *J. Am. Chem. Soc.* **2012**, *134*, 11632−11639.
(51) Yue, L.; Liu, Y.-J. *J. Chem. Theory Comput.* **2013**, *9*, 2300−2312.
(52) Isobe, H.; Takano, Y.; Okumura, M.; Kuramitsu, S.; Yamaguchi, K. *J. Am. Chem. Soc.* **2005**, *127*, 8667−8679.
(53) Watanabe, N.; Kikuchi, M.; Maniwa, Y.; Ijuin, H. K.; Matsumoto, M. *J. Org. Chem.* **2010**, *75*, 879−884.
(54) Koo, J.-Y.; Schuster, G. B. *J. Am. Chem. Soc.* **1977**, *99*, 6107−6109.
(55) Ciscato, L. F. M. L.; Bartoloni, F. H.; Weiss, D.; Beckert, R.; Baader, W. J. *J. Org. Chem.* **2010**, *75*, 6574−6580.
(56) Bastos, E. L.; da Silva, S. M.; Baader, W. J. *J. Org. Chem.* **2013**, *78*, 4432−4439.
(57) Ishii, Y.; Hayashi, C.; Suzuki, Y.; Hirano, T. *Photochem. Photobiol. Sci.* **2014**, *13*, 182−189.
(58) Sun, Y.; Ren, A.-M.; Li, Z.-S.; Min, C.-G.; Ren, X.-F.; Feng, J.-K. *Chem. J. Chin. Univ.* **2011**, *32*, 2586−2592.
(59) Yue, L.; Roca-Sanjuán, D.; Lindh, R.; Ferré, N.; Liu, Y.-J. *J. Chem. Theory Comput.* **2012**, *8*, 4359−4363.
(60) Cohen, A. J.; Mori-Sánchez, P.; Yang, W. *Science* **2008**, *321*, 792−794.
(61) Dreuw, A.; Head-Gordon, M. *J. Am. Chem. Soc.* **2004**, *126*, 4007−4016.
(62) Dreuw, A.; Weisman, J. L.; Head-Gordon, M. *J. Chem. Phys.* **2003**, *119*, 2943−2946.
(63) Yanai, T.; Tew, D. P.; Handy, N. C. *Chem. Phys. Lett.* **2004**, *393*, 51−57.
(64) Stratmann, R. E.; Scuseria, G. E.; Frisch, M. J. *J. Chem. Phys.* **1998**, *109*, 8218−8224.
(65) Casida, M. E.; Jamorski, C.; Casida, K. C.; Salahub, D. R. *J. Chem. Phys.* **1998**, *108*, 4439−4449.
(66) Bauernschmitt, R.; Ahlrichs, R. *Chem. Phys. Lett.* **1996**, *256*, 454−464.
(67) Hehre, W. J.; Ditchfield, R.; Pople, J. A. *J. Chem. Phys.* **1972**, *56*, 2257−2261.
(68) Hariharan, P. C.; Pople, J. A. *Theor. Chim. Acta* **1973**, *28*, 213−222.
(69) Barone, V.; Cossi, M. *J. Phys. Chem. A* **1998**, *102*, 1995−2001.
(70) Cossi, M.; Rega, N.; Scalmani, G.; Barone, V. *J. Chem. Phys.* **2001**, *114*, 5691−5701.

DOI: 10.1021/ct5009203
J. Chem. Theory Comput. 2015, 11, 591−599

(71) Cossi, M.; Rega, N.; Scalmani, G.; Barone, V. *J. Comput. Chem.* **2003**, *24*, 669−681.
(72) Frisch, M. J.; Trucks, G. W.; Schlegel, H. B.; Scuseria, G. E.; Robb, M. A.; Cheeseman, J. R.; Scalmani, G.; Barone, V.; Mennucci, B.; Petersson, G. A.; Nakatsuji, H.; Caricato, M.; Li, X.; Hratchian, H. P.; Izmaylov, A. F.; Bloino, J.; Zheng, G.; Sonnenberg, J. L.; Hada, M.; Ehara, M.; Toyota, K.; Fukuda, R.; Hasegawa, J.; Ishida, M.; Nakajima, T.; Honda, Y.; Kitao, O.; Nakai, H.; Vreven, T.; Montgomery, J. A., Jr.; Peralta, J. E.; Ogliaro, F.; Bearpark, M.; Heyd, J. J.; Brothers, E.; Kudin, K. N.; Staroverov, V. N.; Kobayashi, R.; Normand, J.; Raghavachari, K.; Rendell, A.; Burant, J. C.; Iyengar, S. S.; Tomasi, J.; Cossi, M.; Rega, N.; Millam, J. M.; Klene, M.; Knox, J. E.; Cross, J. B.; Bakken, V.; Adamo, C.; Jaramillo, J.; Gomperts, R.; Stratmann, R. E.; Yazyev, O.; Austin, A. J.; Cammi, R.; Pomelli, C.; Ochterski, J. W.; Martin, R. L.; Morokuma, K.; Zakrzewski, V. G.; Voth, G. A.; Salvador, P.; Dannenberg, J. J.; Dapprich, S.; Daniels, A. D.; Farkas, Ö.; Foresman, J. B.; Ortiz, J. V.; Cioslowski, J.; Fox, D. J. *Gaussian 09*; Gaussian, Inc.: Wallingford, CT, 2009.
(73) O'Neal, H. E.; Richardson, W. H. *J. Am. Chem. Soc.* **1970**, *92*, 6553−6557.
(74) De Feyter, S.; Diau, E. W. G.; Scala, A. A.; Zewail, A. H. *Chem. Phys. Lett.* **1999**, *303*, 249−260.
(75) Møller, K. B.; Zewail, A. H. *Chem. Phys. Lett.* **1998**, *295*, 1−10.
(76) Zhong, D.; Zewail, A. H. *J. Phys. Chem. A* **1998**, *102*, 4031−4058.
(77) Pedersen, S.; Herek, J. L.; Zewail, A. H. *Science* **1994**, *266*, 1359−1364.
(78) Greenman, L.; Mazziotti, D. A. *J. Chem. Phys.* **2010**, *133*, No. 164110.
(79) Foley, J. J.; Rothman, A. E.; Mazziotti, D. A. *J. Chem. Phys.* **2011**, *134*, No. 034111.
(80) Roca-Sanjuán, D.; Lundberg, M.; Mazziotti, D. A.; Lindh, R. *J. Comput. Chem.* **2012**, *33*, 2124−2126.
(81) Vysotski, E. S.; Lee, J. *Acc. Chem. Res.* **2004**, *37*, 405−415.

DOI: 10.1021/ct5009203
J. Chem. Theory Comput. 2015, 11, 591−599